2023-12-01

Viability of Magnetic Nanoparticles for Magnetic Hyperthermia Cancer Therapy

Marcos Adrian Garcia
University of Texas at El Paso

VIABILITY OF MAGNETIC NANOPARTICLES FOR

MAGNETIC HYPERTHERMIA

CANCER THERAPY

MARCOS ADRIAN GARCIA

MASTER'S PROGRAM IN PHYSICS

APPROVED:

_____

Ahmed A. El-Gendy, PhD., Chair

_____

Mark R. Pederson, PhD.

_____

Sylvia L. Natividad-Diaz, PhD.

_____

Stephen L. Crites, Jr., PhD.

Dean of the Graduate School

Dedication

I want to dedicate this thesis to my family, who have always supported me in pursuing what I love. I want to also dedicate this to my friends and lab mates, because without them I would not working in the lab would have been so much harder. Thank you!

“The Highest forms of understanding we can achieve are laughter and human compassion.”

-Richard Feynman

VIABILITY OF MAGNETIC NANOPARTICLES FOR MAGNETIC HYPERTHERMIA CANCER THERAPY

BY

MARCOS ADRIAN GARCIA

THESIS

Presented to the Faculty of the Graduate School of
The University of Texas at El Paso
in Partial Fulfillment
of the Requirements
for the Degree of

MASTER OF SCIENCE

Department of Physics
THE UNIVERSITY OF TEXAS AT EL PASO
December 2023

Acknowledgements

I want to start by thanking Dr. Ahmed A. El-Gendy for giving me the opportunity to join his research lab back in the Fall of 2021. Being able to be part of his lab has allowed me to experience new things and get involved with experimental work. I was able to find interests that I did not think I had in the field of medicine, biology, chemistry and materials science. He has been an awesome mentor who was always there to support me in every step of the way this past two years. He was not only a great mentor but a great friend.

I want to thank everyone in the Nanoland and Biomagnetics lab as well. Without them this work would not have been possible. Thanks to former members of our lab as well such as Jennifer DeAlba and Siria Lee Jansen who were great friends to me, made working in the lab more fun that it should be and were always willing to help me with my work. Thanks to Yohannes Getahun for having the patience to teach me the ins and outs of the lab and the chemistry part of it and always being a good listener. I would also like to thank one of our newest members in the lab, Mariam Elabbasi for making this last semester of my master's enjoyable and for the help she has provided to me.

The Physics Department which I have shared both my undergraduate and graduate careers with. More specifically I would like to thank Dr. Sergio Flores, Karla Carmona, Elyana Amparan for always lending a helping hand when needed and being the best supporters during my masters. I have learned a lot from all of you. I was able to be a TA and learned a lot, I really enjoyed teaching physics labs and being able to share my knowledge with my students. Being part of the Physics Circus also provided me with new experiences and teach high school, middle school and

elementary kids the fun concepts in Physics. My classmates who struggled along with me to do homework and study for exams, I will be eternally grateful for your help.

The last group of people I would like to acknowledge and give thanks too from the bottom of my heart is my family. They were the ones that pushed me to keep going when things got difficult. Always supporting me in any way possible and the reason why I always wore a smile on my face. I love you all! Thank you!!

Table of Contents

List of Tables

List of Figures

Chapter 1: Introduction

In the past two decades nanoscience and nanotechnology has been rapidly expanding and has become an interest of research in all areas in the scientific community [1]. Magnetic nanoparticles (MNP's) have garnered much attention over the years due to their diverse use in biomedicine such as MRI, drug delivery, and cancer therapy. Magnetic hyperthermia has been the focus of many biomedical researchers due to its potential as a cancer treatment that kills the cancer cells with little side effects to the patient. Currently, nanomagnetic research has focused on the use of iron-oxide nanoparticles for hyperthermia applications. However, bimetallic nanoparticles have become an innovative approach to use in biomedicine. [2-5]. Due to their high susceptibility to heat and its high magnetic properties, there has been an interest in producing pure iron nanoparticles.

The introductory chapter will provide the reader with a background into the theories on which this science is established. It will cover topics such as magnetism with a focus on the hysteresis curves, relaxation and the type of magnetic materials that can be related to the application of magnetic heating. The focus of this thesis will be Fe@Ag magnetic nanoparticles as well as FeCo@C magnetic nanoparticles, the synthesis, characterization, their magnetic properties, and their applications for magnetic hyperthermia cancer therapy.

1.1. Nanoscience

It was Nobel laureate and physicist Richard Feynman that first introduced us to the idea of miniaturization in his 1959 lecture "There's Plenty of Room at the Bottom" [6]. With this, interest in the world at a nanoscale started to increase in the scientific community. It wasn't until the 1970's that the word "nanotechnology' was first coined by Professor Norio Taniguchi to the production of materials at the nanoscale [7]. The eighties brought forth a surge in nanotechnology research and it was also during this period that the word "nanoparticle" was introduced into the dictionary [8].

The term "Nanoparticle" refers to a particle within the size range of 1-100 nm [9]. Figure 1 gives a visual representation of the nanoscale to gain a better understanding of the scale[11]. The increase development of materials at the nanoscale provides an important increase in all research areas in the scientific community, technology, and in our daily lives.

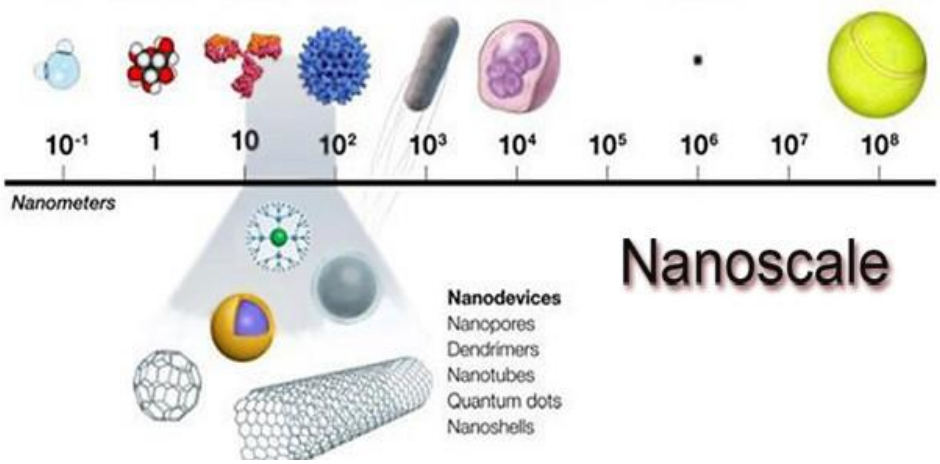

Fig 1: Representation of the Nanoscale

The essence and promise of nanoscience and nanotechnology come from the fact that the physical, chemical, and biological properties of a material be different at the nanoscale from the bulk material [10]. Nanoparticles have been around for quite some time now, from the Lycurgus cup that contains gold, silver and copper nanoparticles that when it interacts with light allow it to produce two colors (green and red-purple in transmitted light). To a more recent discovery of carbon dots (C-dots) that were discovered by Xu in 2004 [11].

As mentioned, nanoparticles provide a wide range of uses in science, especially magnetic nanoparticles (MNP's). One important area would be biomedicine and its applications to magnetic resonance imaging (MRI), drug delivery, and magnetic hyperthermia. Before jumping into how magnetic nanoparticles contribute to these areas, we must first understand the magnetic properties and behaviors they possess to maximize their usefulness in different areas.

1.2. Magnetic Nanoparticles

As mentioned before, interest in nanoparticles has increased over the past decades and their applications has reached all research areas. In recent years one the fields it has made a great impact on is biomedicine. With the versatility that nanoparticles provide in biomedicine it has become a popular research interest in drug delivery, hyperthermia and even MRI [2-5]. When it comes to magnetic nanoparticles in this field, the most typical system that can be found is Fe_3O_4. With its high magnetic properties and its simple and versatile production method it has been researched in almost all applicable fields with great results. Although a great system, core/shell systems have also increased

in popularity in recent years for the extra properties it provides to iron system. This will be discussed further in section 1.3.2. With this we will explore the advantages of using pure iron in a system.

1.2.1. Iron Particles

Iron oxide nanoparticles have been used in many applications for some time now due to the high magnetic saturations they are able to produce and their simplicity in synthesizing them. Although their applications are many, due to the oxide present they will not reach higher values than 100 emu/g. Pure iron particles have the advantage of being able to reach magnetic saturation values that are close to bulk (217.6 emu/g) [22]. With these high values their applications in MRI technology and hyperthermia cancer therapy are desired.

1.2.2. Core/Shell

The term Core/Shell refers to a system in which a material is used as a core and coated with another material on top of it. Doing this can have its advantages in many fields. For example, doing this in the field of biomedicine can reduce the cytotoxicity of particles and increase their dispersion. It can also increase thermal and chemical stability in treatments like hyperthermia cancer therapy [23]. The increase of dispersion and the reduction of cytotoxicity of nanoparticles makes this type of system a very sought out for drug delivery. Advantages of having Core/Shell system with an Iron particle is that the shell material will protect the iron particle from oxidation allowing for the iron

particle to maintain its high magnetic properties. In the case of hyperthermia cancer therapy, materials like gold and silver can introduce the advantages of being great heat conductors and increasing the temperature at a much faster rate.

1.3. Magnetism

Magnetism has been known for centuries. The first material that was found to be magnetic was magnetite (Fe3O4), in ancient Greece. It can be defined as a force exerted by magnets that either attracts or repels. At a more fundamental level, it can be described as the motion of electric charges that when they spin, they create a magnetic dipole [12].

The best way to imagine a magnetic dipole is to see it as a microscopic bar magnet. It is a vector quantity where the magnetic dipole moment is parallel to the electric dipole moment and the direction of the magnetic moment is from south to north. For a material, there are two magnitudes that determine their magnetic moments, this is M and J. M can be represented as $\frac{dM}{dV}$ (A/m), which represents the magnetic dipole moment per unit volume. J is the magnetic polarity of a material and can be described by the equation $J = \mu_0 \frac{dM}{dV} = \mu_0 M$. Where μ_0 represents the magnetic field constant 4πx10^{-7}H/m.

1.3.1. Hysteresis

Hysteresis comes from the Greek word “hyst´er¨esis” -delay, which means that the value describing some physical process is ambiguously dependent on an external parameter and antecedent history of that value must be taken into account. In magnetism and electricity, it descibes the first order phase transition of a material. It can be seen in hysteresis loops where it

measures the magnetization M of magnetic field B against the magnetic field intensity H. Equation 1 shows the magnetic field in a vacuum to be

$$\boldsymbol{B} = \boldsymbol{\mu_0 H}$$

where if the material was present the equation becomes

$$\boldsymbol{B} = \boldsymbol{\mu_r \mu_0 H}$$

where $\boldsymbol{\mu_r}$ represents the relative permeability of the material. The value $\boldsymbol{\mu_r}$ is dimensionless and is just represented by a number that characterizes the material. With this we can get the relationship to be.

$$\boldsymbol{B} = \boldsymbol{\mu_0 (H + M)}$$

Hysteresis curves can also be referred to as M-H graphs. When the applied magnetic field is increased from zero, the magnetic moments of the material become aligned with the magnetic field. When this happens, the magnetic moments of the material will all be aligned, and its maximum saturation value will be obtained [13]. At the maximum saturation value, the applied field changes direction but the values of the magnetization match the previous values but negatively. The value on the y axis at which x = 0 is known as the remanent magnetization. The same for the value at x where y = 0 is the coercivity, and this is the strength of the applied magnetic field required to bring the magnetization of the sample to zero after it has been fully saturated in one direction. The value represented by the coercivity is what defines a material as being a hard magnet of a soft magnet.

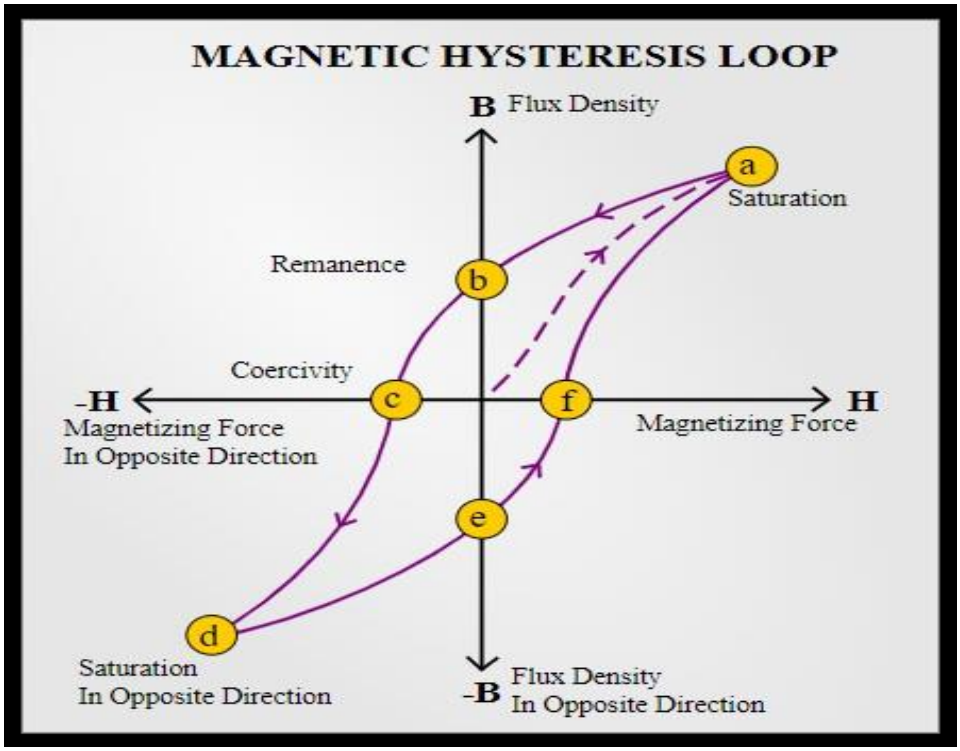

Figure 2: Hysteresis loop representation

Depending on whether you are dealing with a hard or soft magnet, the size of your hysteresis and coercivity will be dependent on this. The coercivity and remanent magnetization will be dependent on grain size, for a hard magnet, which are single domain particles, the magnetization must be reversed to get high coercivities and bigger hysteresis loops. As for a soft magnet, they will have lower coercivities with a smaller hysteresis loop [14].

1.3.2. Relaxation

The approach of a magnetic moment to its equilibrium or steady state as the magnetic field is changed is known is known as relaxation or magnetic relaxation. There are two types of magnetic relaxation, Neel relaxation and Brownian relaxation. The relaxation time of both the

Neel and Brownian are typically related to the anisotropy energy, hydrodynamic size and viscosity of the liquid [16].

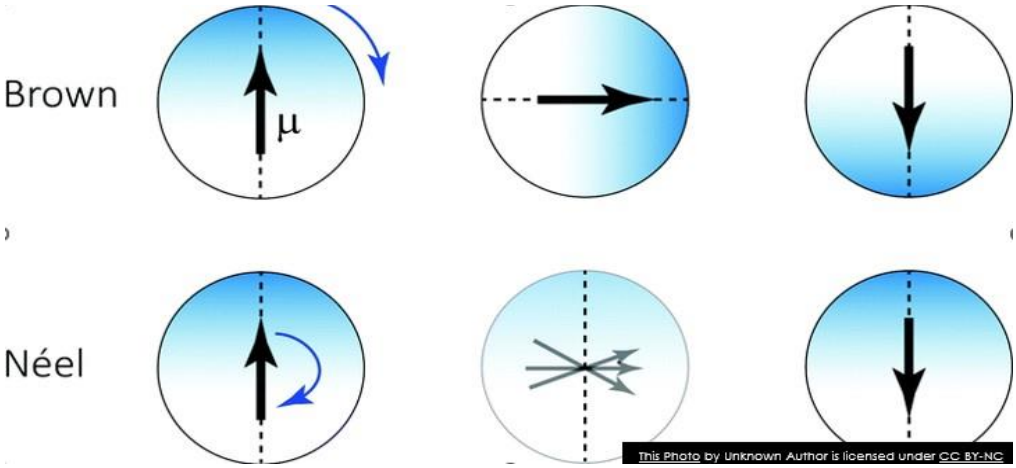

Figure 3: Neel-Brownian relaxation representation

Neel relaxation is when the magnetic vector inside a core realigns itself against the energy barrier [17]. For Neel relaxation the time constant it takes for the particle to stabilize is dependent on the particle size and is often represented as an exponential function called the Neel-Arrhenius equation

$$\boldsymbol{\tau_N = \tau_0 e^{(\frac{KV}{k_B T})}}$$

where τ_0 represents $10^9 - 10^{-10}$s, k_B the Boltzmann constant, K the anisotropy, T the temperature and V the particle volume [18].

Brownian relaxation is when a particle rotates with the fluid [17]. Unlike Neel relaxation, Brownian relaxation time constant is not so dependent on particle size but on the viscosity of the liquid the particle is in. Brownian relaxation can be represented by the equation

$$\tau_B = \frac{3V}{\boldsymbol{k_B T}}\eta = \frac{\pi D^3}{2\boldsymbol{k_B T}}\eta$$

where V is the hydrodynamic volume of the particle, D is the hydrodynamic particle diameter and η is the dynamic viscosity of the liquid. From this equation we can see that the relaxation time is dependent on how well the particle is able to rotate in the liquid.

1.3.3. Magnetic Materials

Magnetic behavior can be categorized in different groups depending on the value of their magnetic susceptibility. There are six classifications of magnetic behavior, and they are paramagnetism, diamagnetism, ferromagnetism, ferrimagnetism, anti-ferromagnetism, and superparamagnetism. These are the most typical types of magnetic behavior that are seen in materials and as such are going to the ones discussed in the following sections. It is good to note that the classification of each of the magnetic behaviors depends on their magnetic properties, spin, electronic structure and the behavior of the electrons.

1.3.3.1. Paramagnetism

Paramagnetism can be seen in materials that have random orientation for their unpaired electrons. This means that each electron has its own magnetic moment because the weak coupling was overcome by thermal energy. With this the material will be attracted to the magnetic field that is applied and the spins will align with the applied magnetic field. Once the

magnetic field is removed the spin of the electrons will go back to being random removing any magnetization from the material [18]. When the magnetic field is low and its at room temperature, its magnetization will be low due to the thermal energy in its structure that does not allow for the alignment of the of the magnetic moments but when it is at a low temperature the magnetization increases as the effect of the thermal energy is reduced and allows for the magnetic moments to align with the magnetic field.

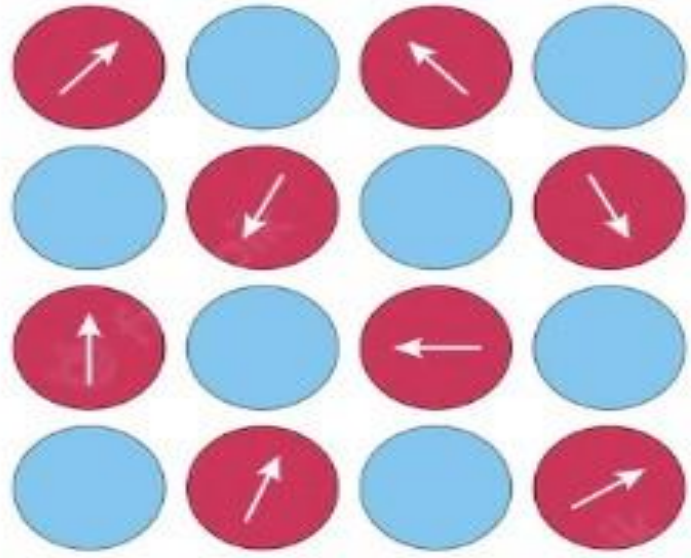

Figure 4: Orientation of Magnetic Moments in Paramagnetism.

1.3.3.2. Diamagnetism

Diamagnetic materials are usually magnetically neutral. This is because they do not have any unpaired electrons like paramagnetic materials. This means that the magnitude of the susceptibility is low and allows for other types of magnetism to take over. One other

characteristic of diamagnetic materials is that they are not affected by the magnetic field or temperature. Because it is considered that it produces a negative magnetization and therefore repels the magnetic field [18].

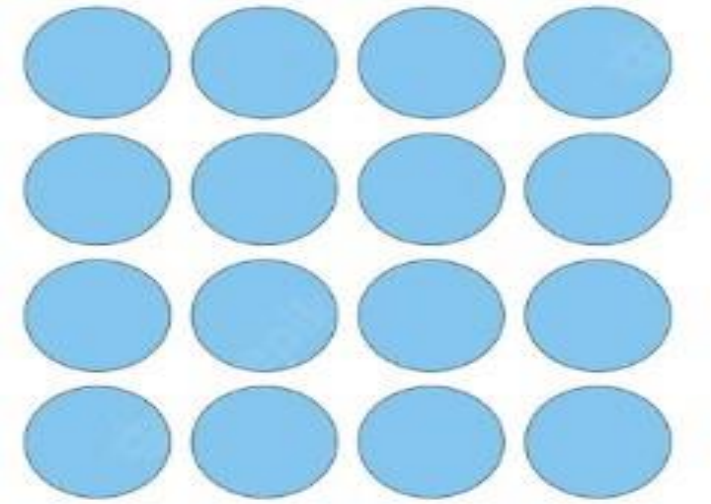

Figure 5: Orientation of Magnetic moments in Diamagnetism.

1.3.3.3. Ferromagnetism

A ferromagnetic material is one that has magnetic forces much higher than that of paramagnetic and diamagnetic materials [19]. Ferromagnetic materials tend to demonstrate high magnetic properties and their hysteresis loops can be described by Figure 2. Although Ferromagnets tend to have stronger magnetic properties than the aforementioned materials once they reach their Curie temperature, T_C, they lose their permanent magnetic properties and become paramagnetic. Ferromagnets can be classified in two groups, hard and soft. Hard ferromagnets tend to be perfect for

permanent magnets and their hysteresis curves can be large and wide. Soft ferromagnets tend to have a smaller hysteresis and are less wide [18].

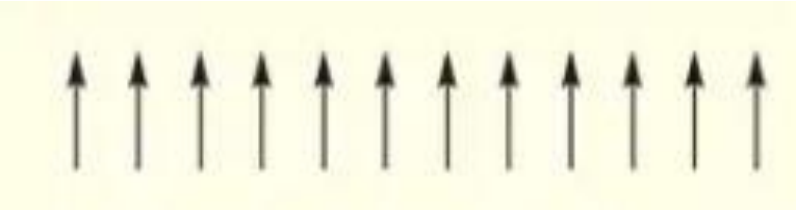

Figure 6: Orientation of ferromagnetism when exposed to a magnetic field.

1.3.3.4. Anti-Ferromagnetism

Anti-Ferromagnetic materials tend to have opposite spins throughout the material, and this makes the material to have almost no gross external magnetism. This is only true when the material is below the Neel temperature, T_N, once it reaches this temperature the heat will interrupt the coupling of the spins. When a magnetic field is applied at low temperatures it will not be affected by the external magnetic field because of the ordering of the spins throughout the material. Once the temperature starts to increase some of the ordering will "break free" and some of the magnetic moments will start to align with the external magnetic field. This will only be true until it reaches the Neel temperature, after this the magnetism of the material will begin to decrease as the temperature increases [18-20].

Figure 7: Orientation of the magnetic moment of anti-ferromagnetism

1.3.3.5. Ferrimagnetism

Ferrimagnetism has the same properties as anti-ferromagnetism. This is that the magnetic moments throughout the material have opposite directions. The difference between the two is that unlike anti-ferromagnetism where the opposing magnetic moments have the same magnitude, in ferrimagnetism the moments do not have the same magnitude. This in turn produces a net magnetic moment. Just like how ferromagnetic and antiferromagnetic materials have a susceptibility to temperature, so does ferrimagnetic materials. This is known as the Ferrimagnetic Neel temperature, T_{FN}, and just like the other two, once it reaches this temperature, the range order of the spins becomes random making the material paramagnetic.

Figure 8: Diagram above demonstrates the orientation and magnitude of a ferrimagnetic material.

1.3.3.6. Superparamagnetism

Superparamagnetic materials are single domain particles which means that particle size will affect its magnetic properties. As the particle size increases, the particle becomes unstable and displays superparamagnetism as a single domain, but an increase in size will make the particle a multi-domain. The macro-spin approximation is when particles with sized less than one hundred nanometers will be single domain particles and the magnetization of this particles can be measured to be one magnetic moment by summing all the individual magnetic moments. When the particles are small, the magnetization can flip and the time in between in each flip where the particle reaches equilibrium is the Neel relaxation time.

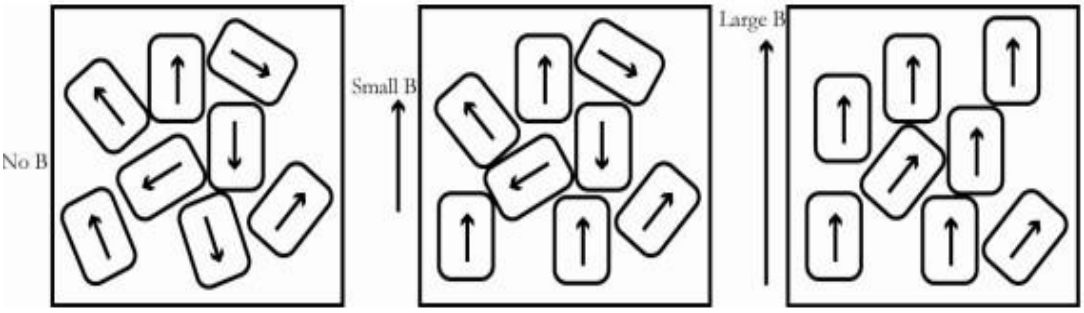

Figure 9: The diagram above demonstrates that when there is no magnetic field the orientation of a superparamagnetic behaves like a paramagnetic. As the magnetic field increases the moments begin to align with the external magnetic field.

One other characteristic of superparamagnetic materials is that they all have a blocking temperature, T_B. When the Neel relaxation time is greater than the measured time, which creates a "blocked state" in the magnetization of the particles and the spin flip does not happen. Vice versa, if the measured time is much greater than the Neel relaxation time the total magnetic moment of the particle will be equal to zero, which produces superparamagnetism. In turn the blocking temperature can be represented by the following equation where the measured time equals the Neel relaxation time.

$$T_B = \frac{KV}{k_B \ln\left(\frac{\tau_m}{\tau_N}\right)}$$

Where τ_m is the measured time and τ_N is the Neel relaxation time. One thing that can be noted is that when the Neel relaxation time is greater than the measured time, the magnetic behavior displayed by the particle will be that of a paramagnetic.

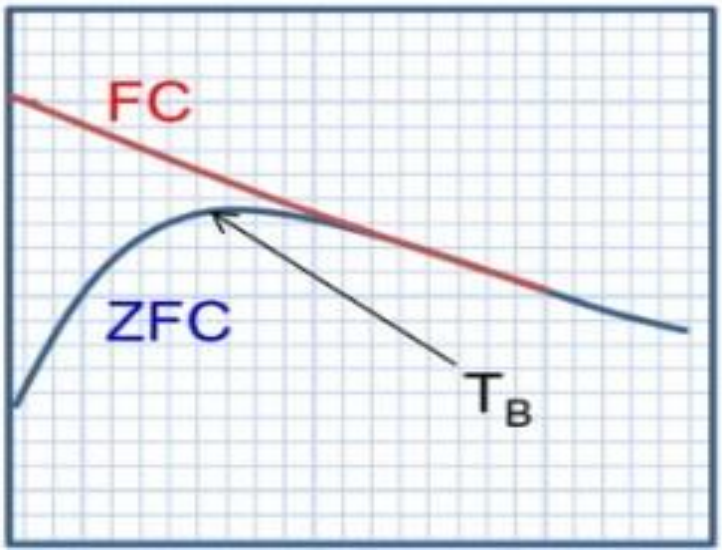

Figure 10: Representation of the blocking temperature where the particle reaches a state of equilibrium. This is when $\tau_N = \tau_m$.

When a magnetic field is applied to a superparamagnetic material the magnetic moments will align with the external magnetic field and will create a net magnetization. As mentioned before the size of the particles will determine the superparamagnetism of a single domain particle. When measuring the M vs H graph of a superparamagnetic it will lose its loop that can be seen in a ferromagnetic, but it will retain a sigmoidal shape it had [21].

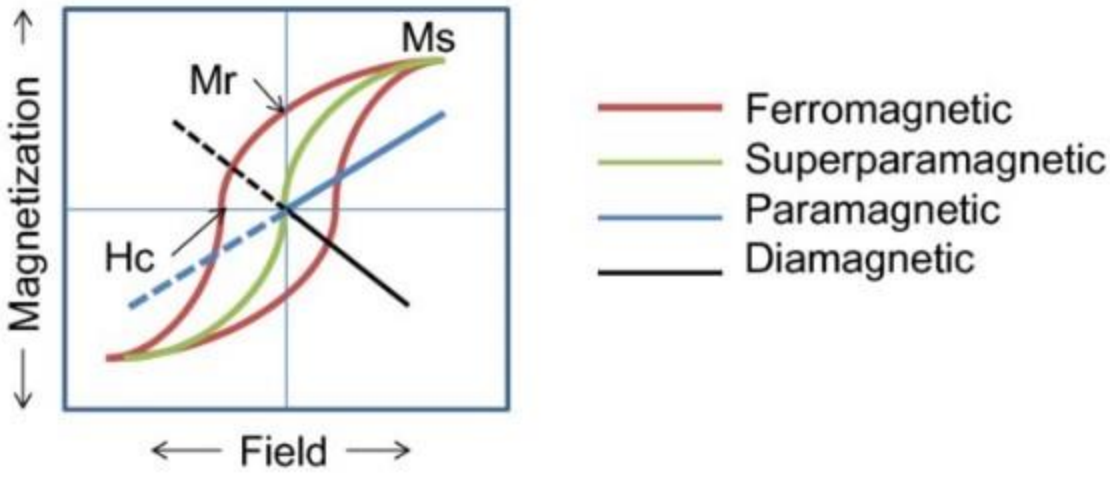

Figure 11: The above MvH of a ferromagnetic, paramagnetic, diamagnetic and a superparamagnetic.

1.4. Magnetic Hyperthermia Cancer Therapy

Hyperthermia can be defined as the technique to increase the body temperature to that of above body temperature. In hyperthermia cancer therapy cancerous cells are exposed to a high temperature to burn and destroy the cancer cells [24]. Hyperthermia cancer therapy can be placed in 3 categories: thermal ablation, moderate hyperthermia and mild hyperthermia. When doing thermal ablation, the temperature the tumor is exposed to is above 45℃ and this cause coagulation or necrosis. A more moderate treatment would be moderate hyperthermia where the temperature the tumor is exposed to is between 40℃ and 45℃. At this temperature the cells will experience stress due to the heat which will result in stopping the reproduction of cells. The last category of hyperthermia, mild hyperthermia, exposes the tumor to temperatures below 40℃ and this is mainly used to make the cells more sensitive to chemotherapy [25].

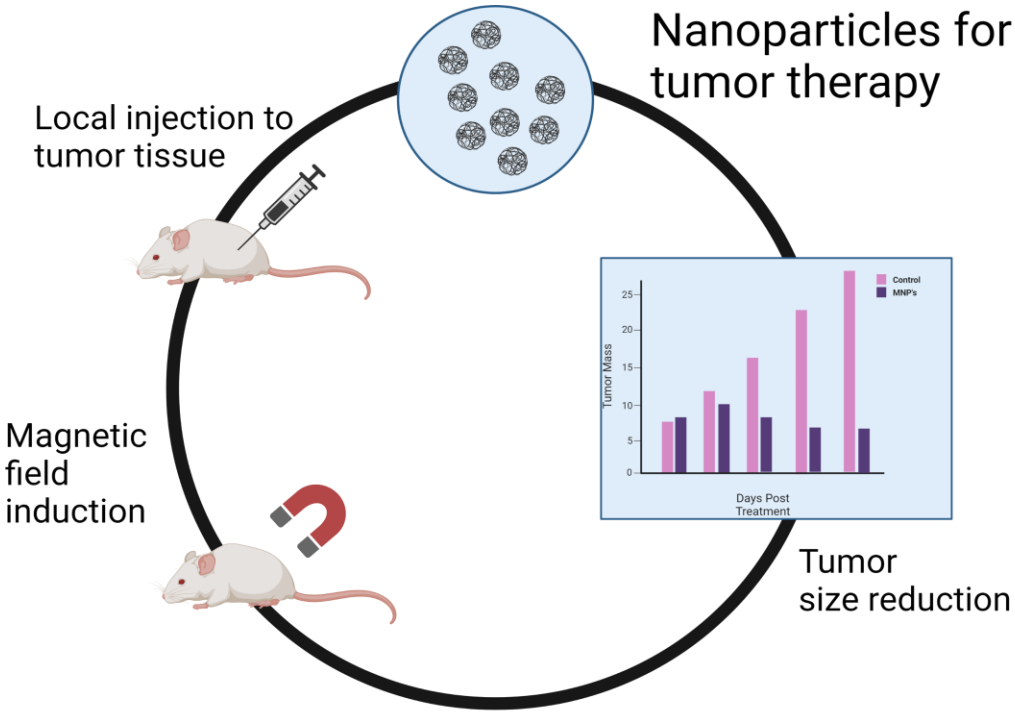

Figure 12: Diagram of Magnetic Hyperthermia Cancer Therapy

In the case of our study, we will be using magnetic nanoparticles to produce heat from inside the tumor and destroy the cancer inside out. The magnetic nanoparticles will be injected directly into the tumor and produce heat by being exposed to an AC magnetic field. With this, we hope to localize the treatment to only cancer cells, as they are more susceptible to heat than healthy cells and keep the healthy cells undamaged. This is one of the challenges hyperthermia cancer therapy faces but depending on the tumor location, it can show promising results. In this study we will analyze two different systems of Core/Shell magnetic nanoparticles through different methods of characterization and test their feasibility for Hyperthermia Cancer therapy.

Chapter 2: Experimental Methods

2.1. Synthesis Methods

2.1.1. Chemical Synthesis of Iron-Silver nanoparticles

To synthesize Iron-Silver nanoparticles we used a 10:1 ratio of Iron (II) Sulfate tetrahydrate and Sodium Citrate respectively. A 2:1 ratio of Iron (II) Sulfate tetrahydrate and Sodium Borohydride, and 0.7mMol of Silver Nitrate all dissolved in 30mL of DI water. The iron precursor and sodium citrate were first placed in a beaker with 20mL of water and stirred magnetically at 1000rpms for 10 minutes to allow them to dissolve. The Sodium Borohydride was dissolved in 10mL of DI water and was added slowly to the iron (II)sulfate and sodium citrate solution after 10 minutes to begin nucleation of the particles. Five minutes after adding the Sodium Borohydride, 1mL of Silver Nitrate is slowly added to the solution and left to stir for 10 minutes. After 10 minutes the solution is quenched with 20mL of ethanol and removed from magnetic stirring. The particles are then cleaned with ethanol, sonicated for 45 minutes then rinsed three more times and left to dry in ambient temperature. This process is repeated for each of the samples synthesized with a Silver Nitrate injection time of 1, 3, 7, 9, 10, 11, 13, and 15 minutes.

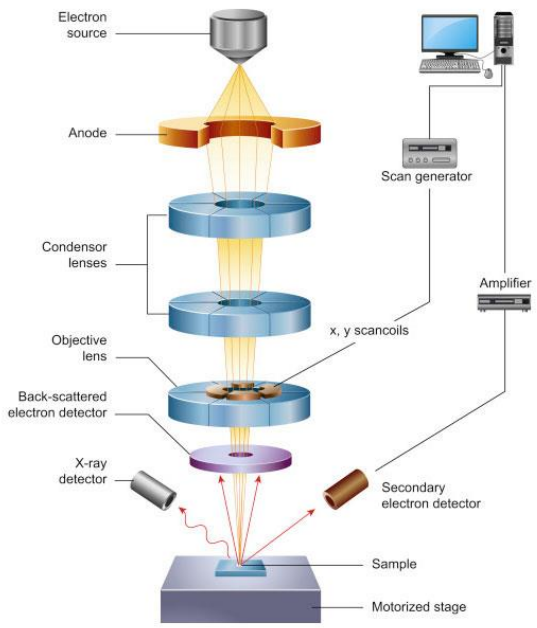

Figure 13: Represents the function of Scanning Electron Microscopy

2.1.2. Chemical Synthesis of Iron-Cobalt nanoparticles

The Chemical synthesis of Iron-Cobalt magnetic nanoparticles was carried out by using a 1:1 ratio of Iron(II)Chloride Tetrahydrate and Cobalt Acetate, and a 1:6 ratio of Iron(II)Chloride Tetrahydrate and Sodium Hydroxide respectively. 50mL of Ethylene Glycol were poured in a spherical flask and left to heat up to desired temperature. Once the desired temperature had been reached the metal salts were added together and five seconds later the Sodium Hydroxide was added. As soon as the reaction happened the temperature was immediately turned off and the solution was left steering magnetically until cool down. Once the solution was cool, the particles were magnetically separated from the Ethylene Glycol and then rinsed with ethanol 4 times. Then the particles were left sonicating for 1 hour to remove any excess Ethylene Glycol

and impurities from the particles. The particles were then rinsed with ethanol for a few more times. The temperatures at which Iron Cobalt was synthesized was 160℃, 170℃, 180℃ and 190℃.

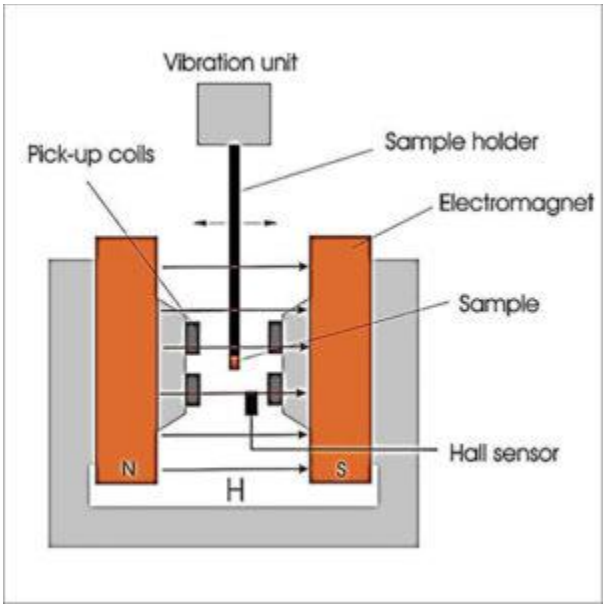

Figure 14: Represents the manner in which VSM collects data regarding the magnetic properties of particles.

2.2. Characterization

2.2.1. Characterization of Iron-Silver and Iron-Cobalt nanoparticles

The crystal structure characterization of the nanoparticles was yielded by PANalytical X'Pert PRO XRD diffractometer with Cu Kα radiation (k = 0.1548 nm). The morphology, particle size and elemental mapping were characterized using scanning electron microscopy (SEM) and the measurements were done using Hitachi S-4800 Field Emission Scanning Electron Microscope (FE-SEM) detector type XFlash 6|60 ex. Equipped with EDX from Bruker Nano GmBH Berlin, Germany. The magnetic properties of the powders were analyzed using a vibrating sample magnetometer (VSM) VersaLab 3 Tesla (VSM) from quantum design. The hysteresis loop,

MxH, was measured at 300 K, with DC magnetic fields up to H=3T. Zero-field-cooling/field-cooling (ZFC/FC) MxT curve was measured from 50 to 400 K. Magnetic Hyperthermia measurements were done using a G2-D5 Series Multi-mode 1500W Driver from Nanoscale Biomagnetics. By placing the powder in a 1mL solution and the respective mass of each sample in a vial that was placed into the G2-D5 coil, an AC magnetic field was introduced at different frequencies and intensities and a fiber optic sensor was used to measure the produced temperature of the particles in the solution.

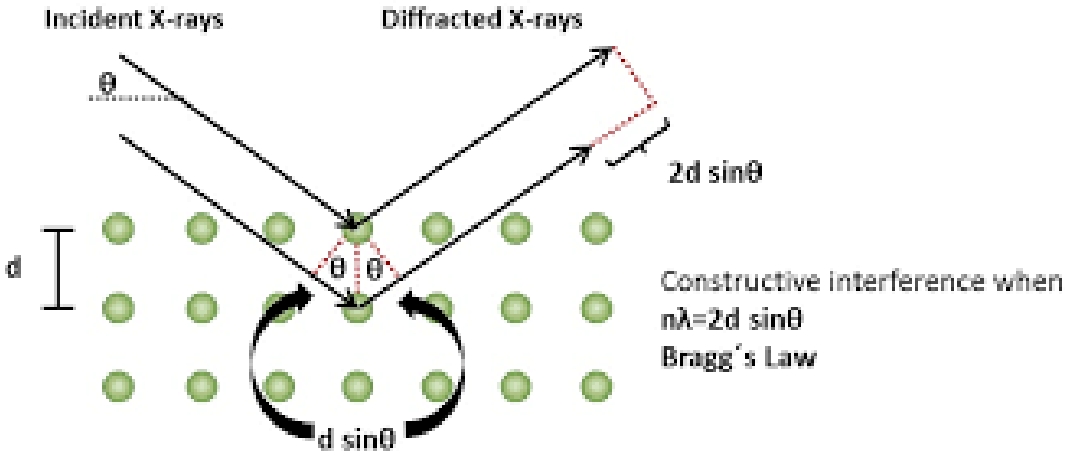

Figure 15: Interaction between X-Rays and molecules to obtain crystal spectrum of materials.

Chapter 3: Iron-Silver Magnetic nanoparticles

3.1. Magnetic Properties

The magnetic properties of the magnetic nanoparticles have been investigated at magnetic fields and temperature of 3T and 300K. In Figure 5 we can see the full hysteresis loop of three samples. For all three samples we can see a superparamagnetic behavior which can be indicated by the closed hysteresis loops. From Figure 4 we can also conclude that it is evident that as the time of injection of the silver precursor varies, so does the magnetic saturation of our nanoparticles. Although after seven minutes we can see a drop in the magnetization. From five minutes to seven minutes, we can see an increase in the magnetization from 163 emu/g to 226 emu/g and then a drop after this at nine minutes to 172 emu/g. This indicates that adding the silver precursor at seven minutes after adding the sodium borohydride provides the most optimal magnetic saturation. Table X shows the different sizes of the particles for size distribution, crystallite size, magnetic domain size and magnetic saturation.

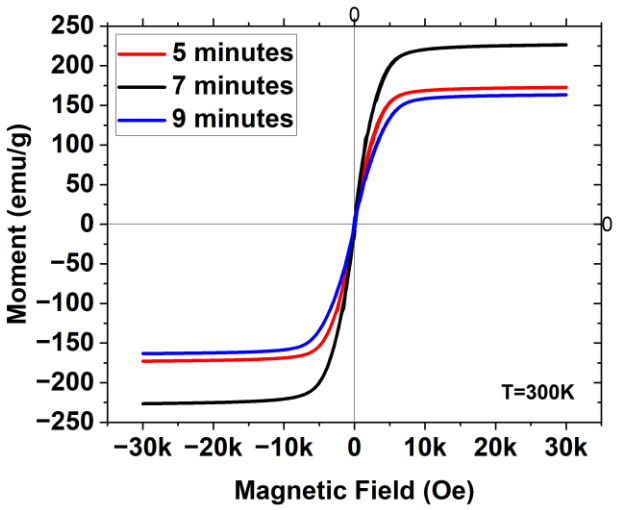

Figure 16. Magnetic Hysteresis loops at different room temperatures (300K) for Iron-Silver.

Table 1: Magnetic Saturation, D_{SEM}, D_{XRD}, and D_{mag} for Iron-Silver nanoparticles.

Sample	M_s	D_{SEM}	D_{XRD}	D_{Mag}
units	**(emu/g)**	**(nm)**	**(nm)**	**(nm)**
5 minutes	172 emu/g	64±20nm	1	3.46
7minutes	226 emu/g	38±9nm	1.4	3.20
9 minutes	163 emu/g	47±13nm	3.6	3.23

Magnetic domain size of the particles was also calculated using Equation (1).

$$Dmag = [\frac{18kBT\frac{dM}{dH}}{\pi\rho Ms^2}]^{\frac{1}{3}}$$

Where Dmag is the magnetic domain size of the particles, kB is the boltzman constant, dM/dH is the slope of the hysteresis curve, π is 3.14, ρ is the bulk density of iron, and Ms is the magnetic saturation. The magnetic domain sized calculated for each of the 5 minute, 7 minute, and the 9 minute samples are 3.46nm, 3.20nm, and 3.23nm respectively.

3.2. Structure and Morphology

The XRD pattern of three samples with different time of injection of silver are shown in Figure 1. The ratios for all three samples were kept at a 2:1 ratio between I(II) Sulfate and Sodium Borohydride and a 10:1 ratio for iron sulfate and sodium citrate respectively. The spectrum demonstrates that our material has corresponding peaks of Fe at around 2θ = 38, 45, and 65. XRD analysis also demonstrates a crystalline structure for this system with crystallite diameters of 1nm-4nm.

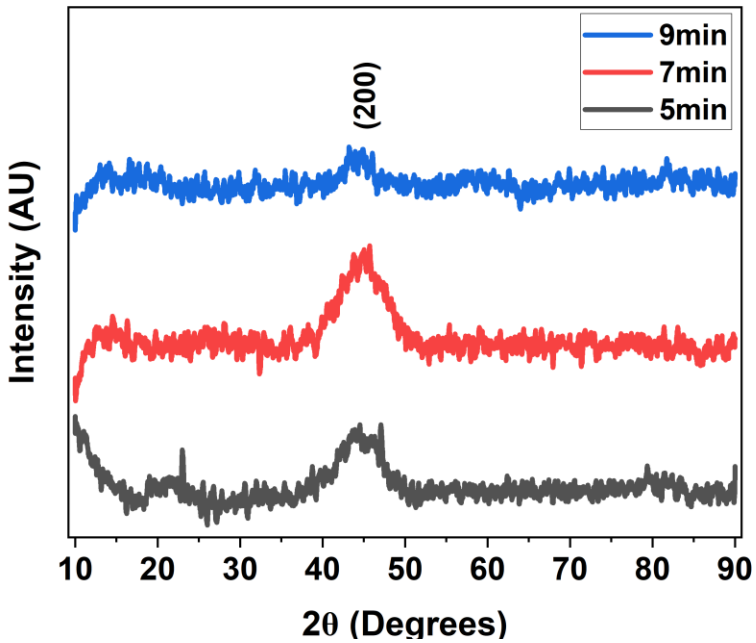

Figure 17: XRD spectrum of Fe-Ag matrix nanoparticles for 3 different times of injection of the silver precursor, 5 minutes (black), 7 minutes (red) and 9 minutes (blue).

This diffraction peaks correspond to the FCC Ag crystal structure and can be confirmed that Iron-Silver was synthesized as the particles demonstrate magnetic properties pertaining to Fe. We can make this assumption because Figure 2 demonstrates traces of iron and silver in our samples. Crystallite size of the nanoparticles was also calculated using Scherer equation using full width at half maximum and is represented by Equation (2).

$$DXRD = \frac{0.93\lambda}{\Delta 2\Theta cos\Theta}$$

Where DXRD is the average crystallite size, λ is the wavelength applied, Δ2Θ is FWHM of the peaks and Θ is Bragg angle. The average crystal size calculated were 1nm, 1.4nm, and 3.6nm respectively for 5min, 7min, and 9min. The values are represented in table 1.

As explained in Chapter 2, the synthesis of Fe-magnetic nanoparticles were done using a chemical reduction method. The sodium borohydride was used as the reducing agent to separate the salts from the metals and the sodium citrate was used as a capping agent as previously reported. This method produced almost homogeneous particles as can be seen by the SEM image in Figure 4. The particles have around the same size and spherical shape although some impurities are still present. Size distribution of the particles was also investigated and from Figure 5 we can see that as the nucleation time changes the size of the particles does as well. A decrease in particles size from five minutes, 64nm, to seven minutes, 38 nm. Then at nine minutes there is a light increase in size to 47 nm. This increase can be attributed to impurities still present in the particles deviating the size distribution of the samples. The sizes displayed in our samples are viable to use in hyperthermia therapy, but smaller particle size is desired.

EDS elemental mapping was also carried out to analyze the elemental components of the samples. As shown in Figure 2 the particles are demonstrated to have great amount of Iron while having some traces of Silver in them among other elements such as Carbon, Oxygen, Sodium and Sulfur that can be considered impurities in the nanoparticles. It can be concluded that the synthesis was successful as the iron particles have some, although very small trace amounts of silver can be found in the particles, it can be assumed that these small traces will contribute to decreasing the time it takes for the magnetic nanoparticles to increase in temperature during magnetic hyperthermia therapy.

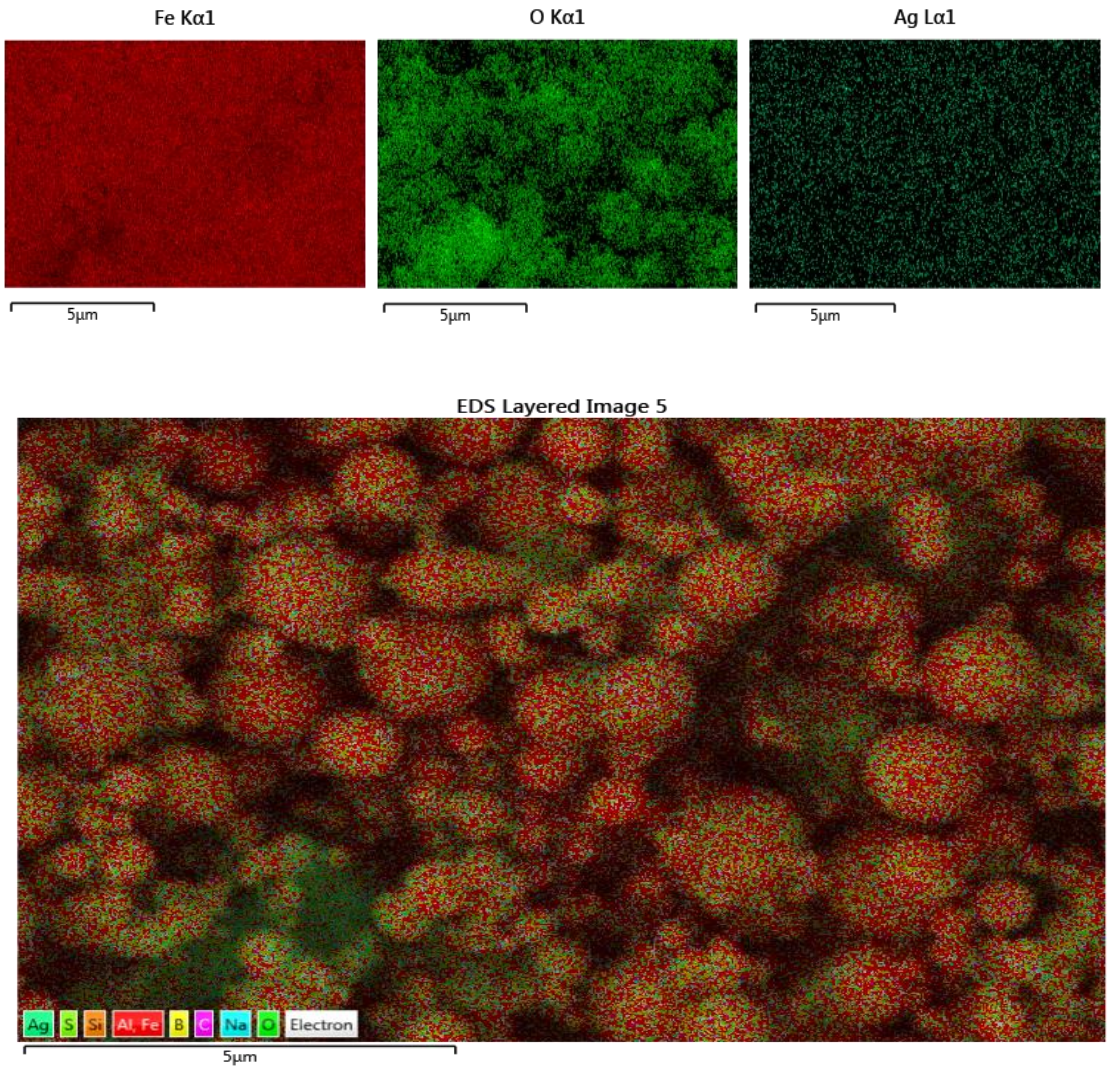

Figure 18. Elemental mapping demonstrates traces of Silver along with other impurities.

EDS and SEM pictures in Figure 2 and 5 also show some impurities in our samples. From EDS we can see that the bigger particles are impurities caused by the reducing agent, NaBH4, during the synthesis of the particles. After SEM and EDS was done the particles were cleaned further using a centrifuge and ethanol to remove these impurities that could later affect our results during the hyperthermia treatment.

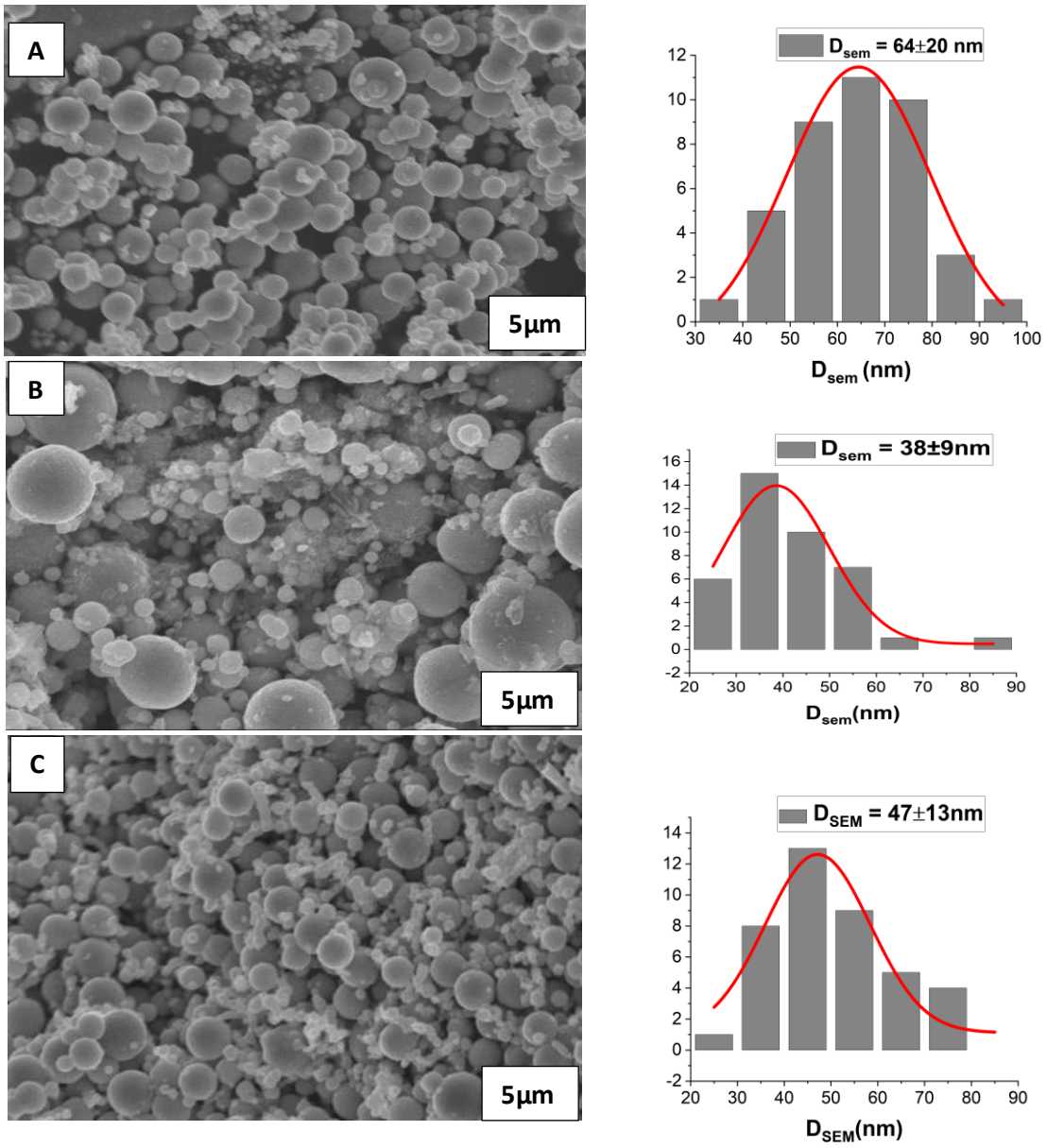

Figure 19. SEM images and size distribution for 5,7, and 9 minutes.

3.3. Hyperthermia

From Figure 3 the time-dependent calorimetric measurements at different applied magnetic field strengths for Iron-Silver are shown. It can be observed that a heating effect is taking place and starting at the magnetic field of 300G to 400G. When the magnetic fields are applied, it can be seen that the heating rate reached values of 3℃/min. Using the specific absorption rate (SAR), which tells us the viability of a material for magnetic hyperthermia applications. The specific absorption rate was calculated using the SAR equation

$$SAR = \frac{C_v m_{total}}{m_{particle}} \frac{dT}{dt}$$

where C_v represents *4.186 J/g*℃*, the specific heat capacity of water, m_{total} the total mass of the sample including water, $m_{particle}$ represents the mass of the sample and $\frac{dT}{dt}$ represents the change in temperature with respect to time. Using this equation, we can see that the SAR increases from 31.99 W/g to 43.49 W/g as the field increases from 300G to 400G. For the all the graphs we can see that at a field of 100G and 200G there is no increase in temperature but as the field increases to 400G the temperature raises and we can see some increase. The only sample that shows no increase in temperature for both 300G and 400G is the sample synthesized at the time of injection of Silver at 9 minutes. SAR graph in Figure XX demonstrates how the heating power produced by all samples at different magnetic fields.

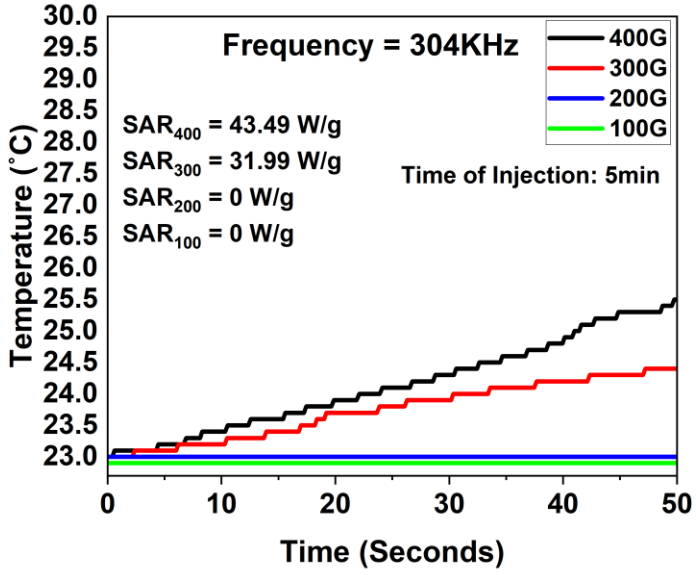

Figure 20: Temperature vs. Time graph of Iron-Silver synthesized with injection of Silver at 5min.

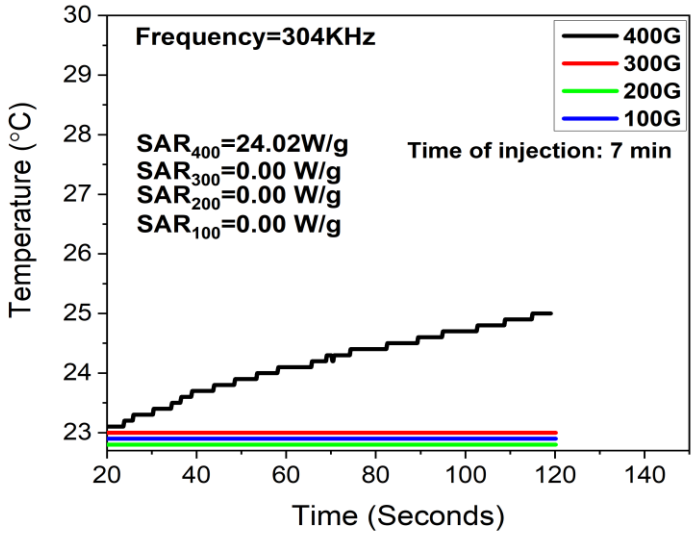

Figure 21: Temperature vs. Time graph of Iron-Silver synthesized with injection of Silver at 7min.

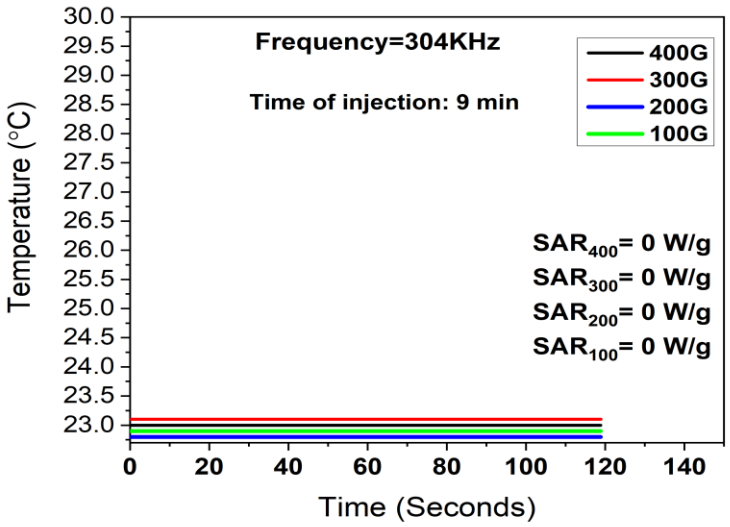

Figure 22: Temperature vs. Time graph of Iron-Silver synthesized with injection of Silver at 9min.

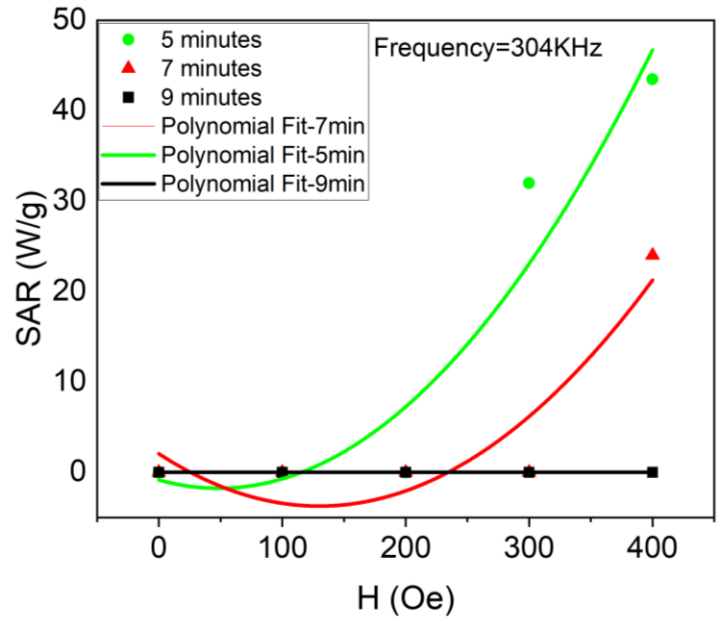

Figure 23: SAR vs magnetic field graph shows that as the field increases, the SAR increases.

Chapter 4: Iron-Cobalt Magnetic Nanoparticles

4.1. Magnetic Properties

The magnetic properties of the Iron Cobalt samples were tested using the Vibrating Sample Magnetometer at an external magnetic field of 3T and at a temperature of 300K. Figure 21 demonstrates the samples to have superparamagnetic behavior at room temperature with magnetic saturations of 84, 25, 101, and 125 emu/g respectively for each of the temperatures of 160℃, 170 ℃, 180 ℃, and 190 ℃.

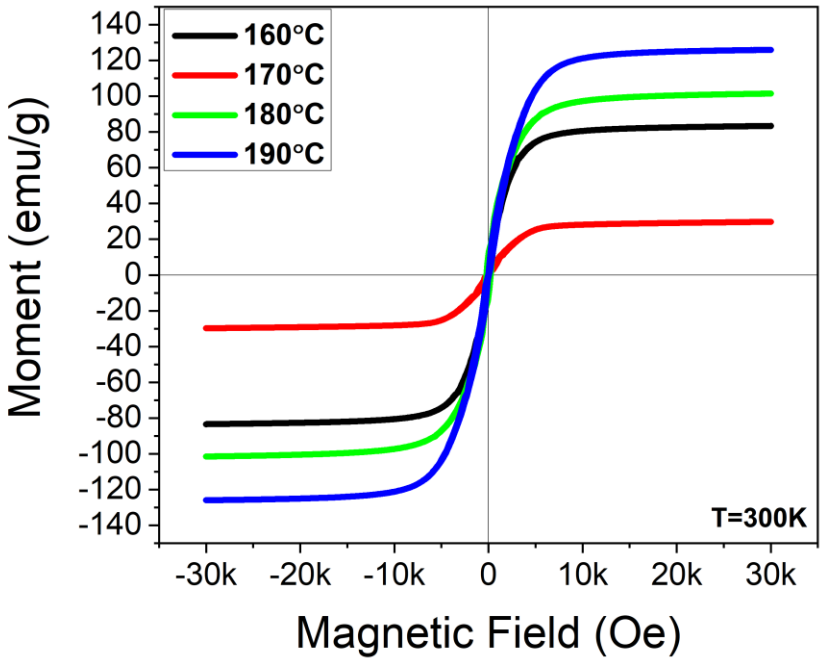

Figure 24: hysteresis curves at room temperature for FeCo synthesized at 160℃, 170℃, 180℃, and 190℃.

4.2. Structure and Morphology

Figure 22 demonstrates the XRD pattern of Iron-Cobalt synthesized at different temperatures. The ratios for all four experiments were kept the same, 1:1 ratio of Iron(II) Chloride Tetrahydride and Cobalt Acetate and a 6:1 ratio of Sodium Hydroxide (pellets) and Iron(II) Chloride Tetrahydrate respectively. It can be seen that the spectrum shows peaks corresponding to FeCo at 45, 65, and 85 degrees for most of the samples where the peaks for FeCo are more clearly defined for the particles synthesized at 170℃.

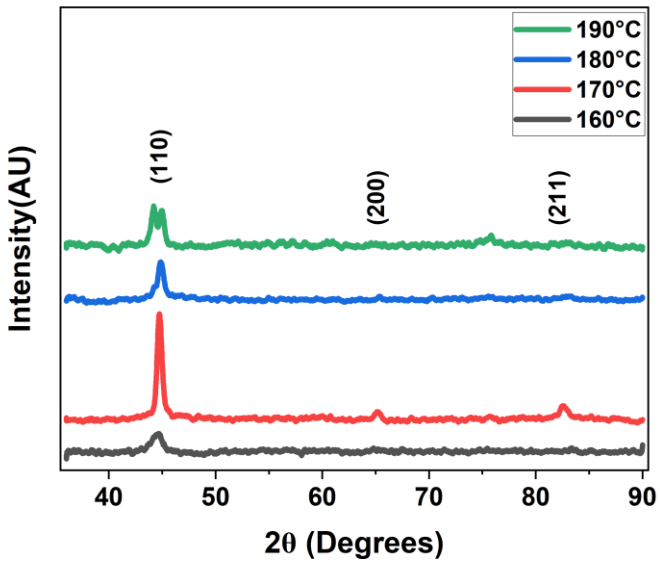

Figure 25: Shows the XRD spectrum for Iron Cobalt synthesized at different temperatures.

Scanning Electron Microscopy and Energy Dispersive X-Ray Spectroscopy were used to study the size and elemental composition of the magnetic nanoparticles. SEM shows a homogeneous distribution in size for all four samples. EDS demonstrates and corroborates the elemental

composition and presence of Iron and Cobalt shown by the XRD spectrum, providing the assurance that chemical synthesis of the particles was successful at 160℃, 170℃, 180℃, and 190℃.

Table 2: Magnetic Saturation and average size distribution for Iron-Cobalt synthesized at different temperatures.

Temperature	Ms	D_{SEM}
˚C	emu/g	nm
160	84	15±15
170	27	44±8
180	101	74±15
190	126	50±20

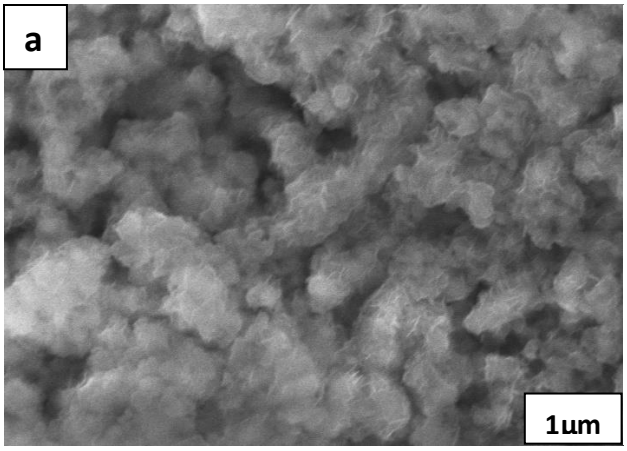
a
1µm

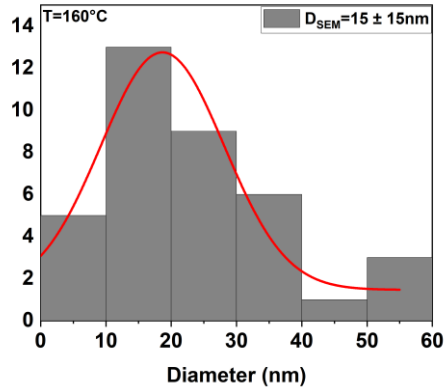
T=160°C
D_{SEM}=15 ± 15nm
Diameter (nm)

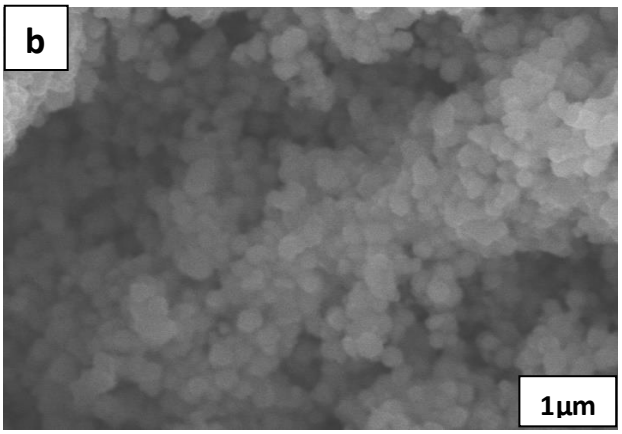
b
1µm

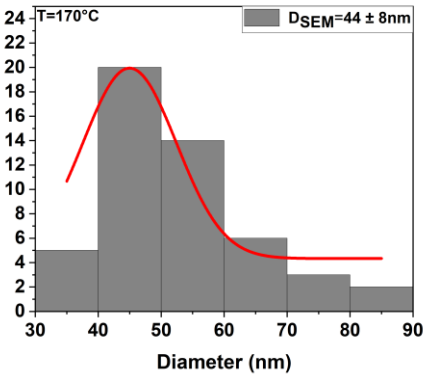
T=170°C
D_{SEM}=44 ± 8nm
Diameter (nm)

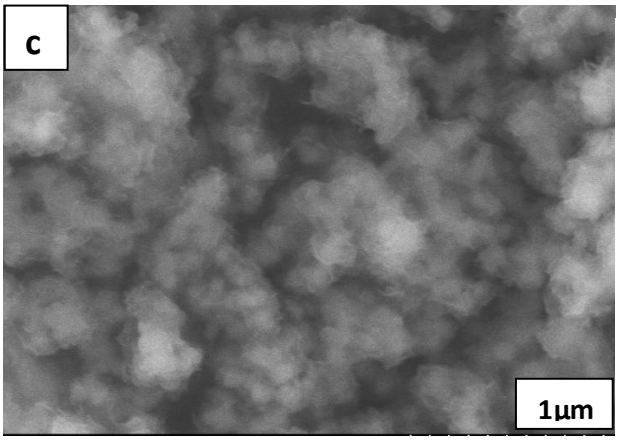
c
1µm

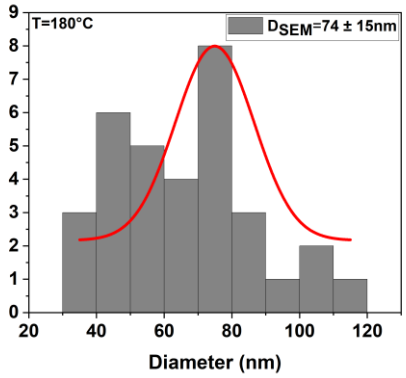
T=180°C
D_{SEM}=74 ± 15nm
Diameter (nm)

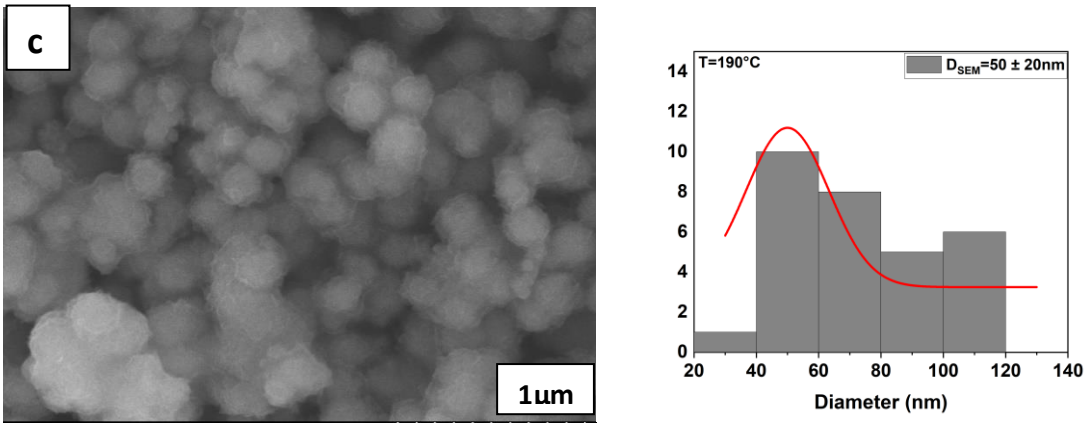

Figure 26: SEM and size distribution of Iron-Cobalt samples synthesized at the temperatures of 160℃, 170℃, 180℃, and 190℃.

Morphology of the Iron-Cobalt nanoparticles was analyzed using Scanning Electron Microscopy and Energy Dispersive Spectroscopy as shown in Figure 23, revealing most of the particles to be of a spherical shape. Size distribution of the magnetic nanoparticles was used to analyze the average size distribution, average size of the particles being 15nm, 44nm, 74nm and 50nm for temperatures of 160℃, 170℃, 180℃, and 190℃ respectively. It can be seen from size calculations that a pattern of an increase in size happens as the temperature increases although this does not happen for the temperature at 190℃. Energy Dispersive Spectroscopy graphs in Figure 24 shows the concentration of each of the elements found in the nanoparticles. It can be seen that EDS further corrobarates the XRD of presence and succesfulness in producing Iron-Cobalt magnetic nanoparticles.

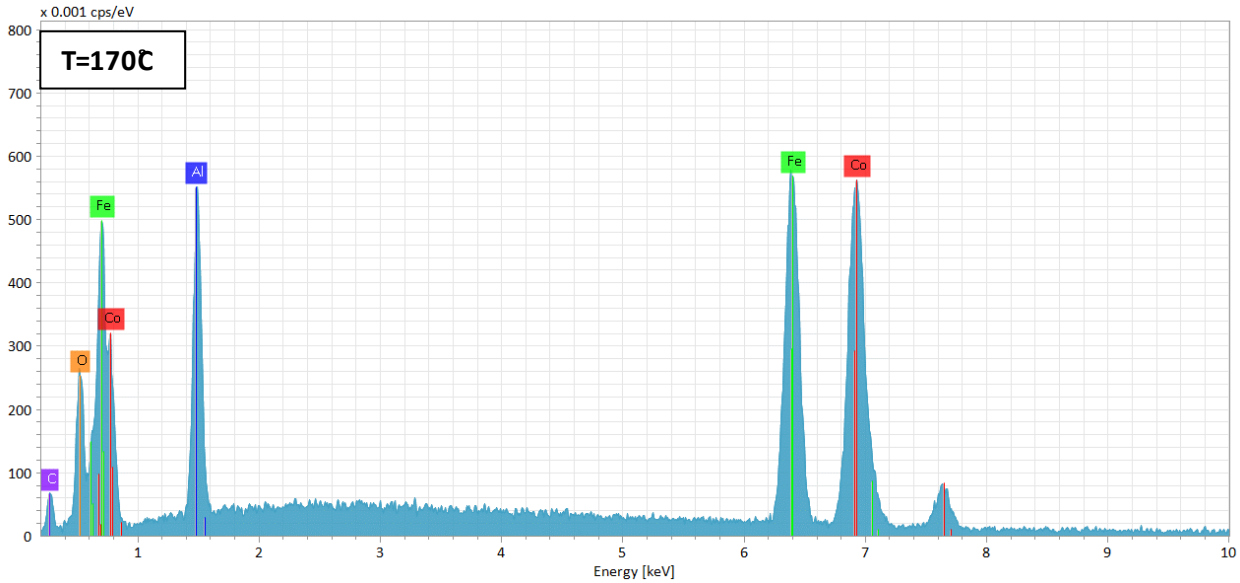
x 0.001 cps/eV
T=170℃
C
O
Fe
Co
Al
Fe
Co
Energy [keV]

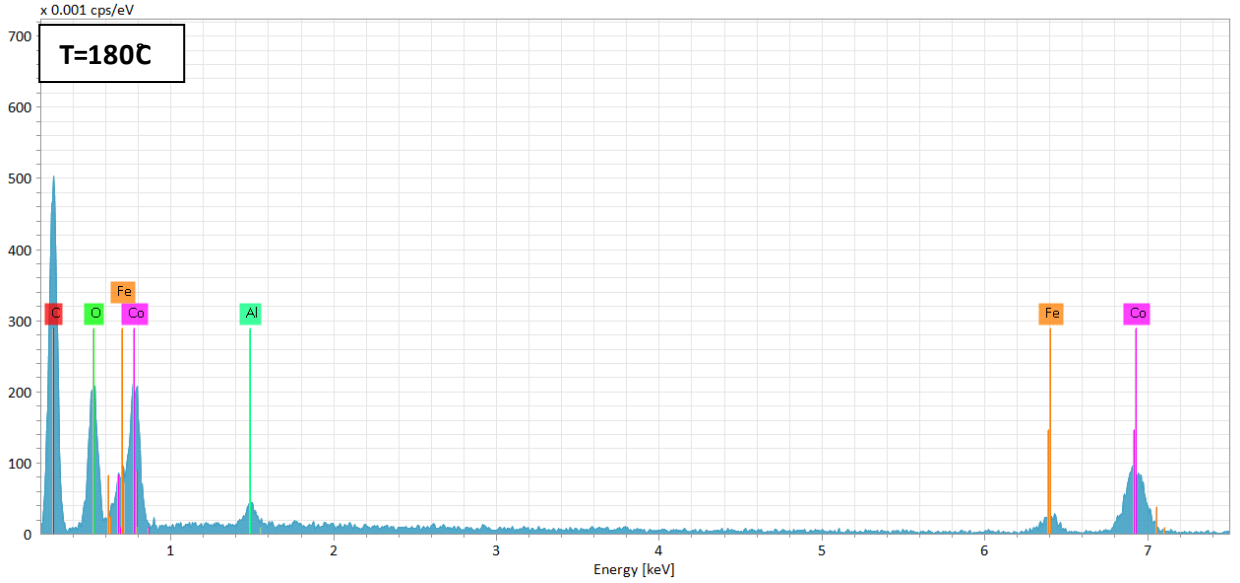
x 0.001 cps/eV
T=180℃
C
O
Fe
Co
Al
Fe
Co
Energy [keV]

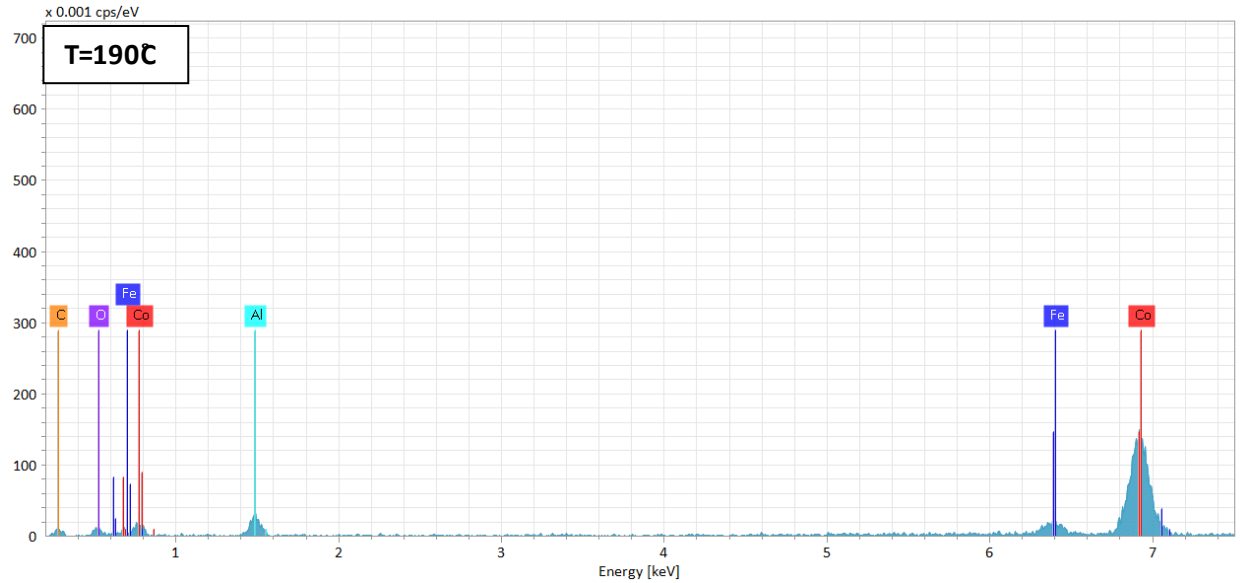

Figure 27: EDS graphs demonstrate the elemental composition of the Iron-Cobalt samples synthesized at different temperatures

4.3. Hyperthermia

Preliminary Hyperthermia results where obtained using the NanoBioMagnetics D5 series Hyperthermia machine. The Iron Cobalt samples were first prepared in small vials with ~5mg/mL concentrations for each one of them. Using a fiber-optic sensor to measure the change in temperature for a certain period of time, the prepared samples were exposed to AC magnetic fields of 300G to 400G with a frequency of 304KHz for 5 minutes. As shown in Figures 25, 25, 27, and 28, for samples with the high magnetic saturation we can see an increase in temperature once the AC magnetic field reached 400G. The one sample with low magnetic properties shows no increase in temperature at all for either 300G and 400G. We can also see that for the FeCo sample synthesized at 190℃, which had the highest magnetic saturation at 125 emu/g, also shows the highest SAR measurement at 400G than the rest of the samples. This can

be seen in Figure 29. This increase in temperature can be due explained by the interaction of the AC magnetic field with the magnetic nanoparticles, the higher the magnetic properties of nanoparticles the faster the rotation of the magnetic moments and the particles.

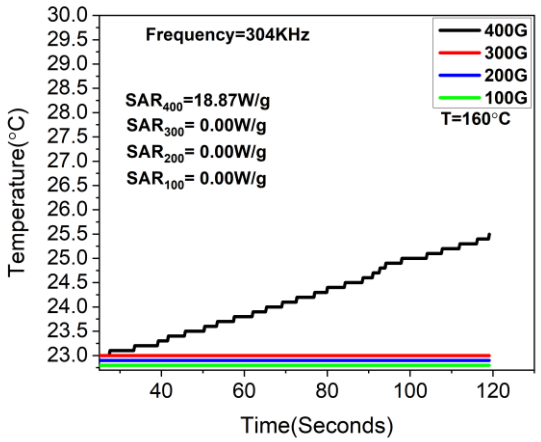

Figure 28: Preliminary results for hyperthermia tests on FeCo magnetic nanoparticles synthesized at 160℃.

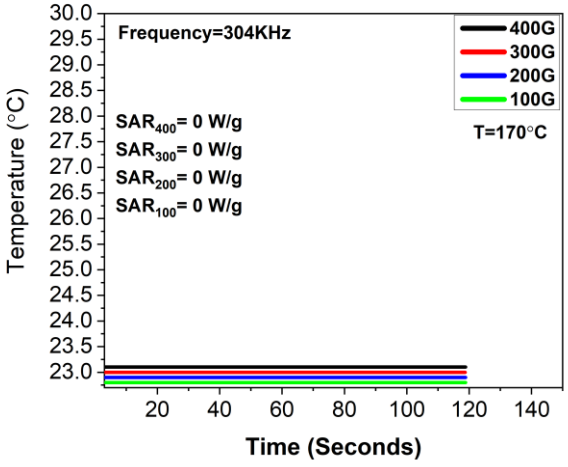

Figure 29: Preliminary results for hyperthermia tests on FeCo magnetic nanoparticles synthesized at 170℃.

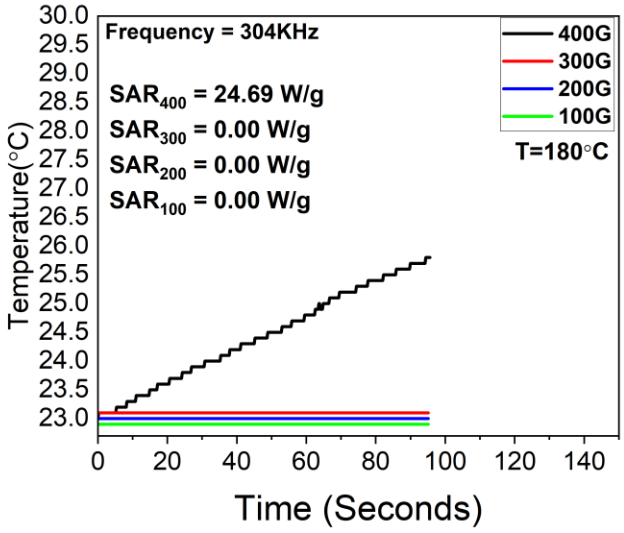

Figure 30: Preliminary results for hyperthermia tests on FeCo magnetic nanoparticles synthesized at 180℃.

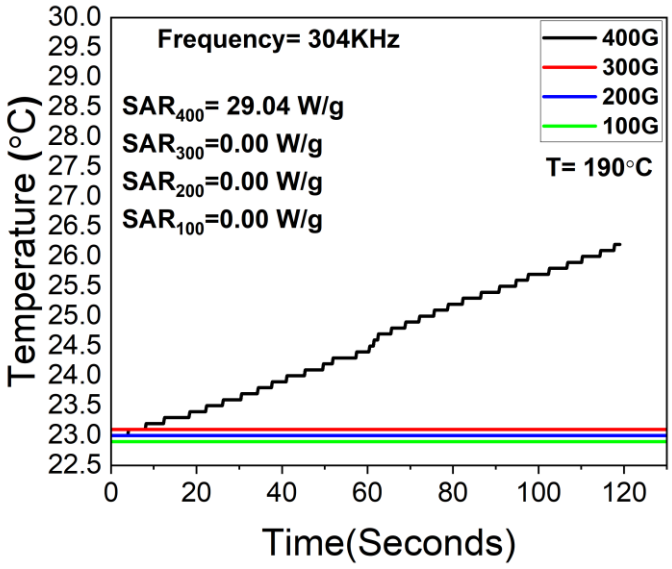

Figure 31: Preliminary results for hyperthermia tests on FeCo magnetic nanoparticles synthesized at 190℃.

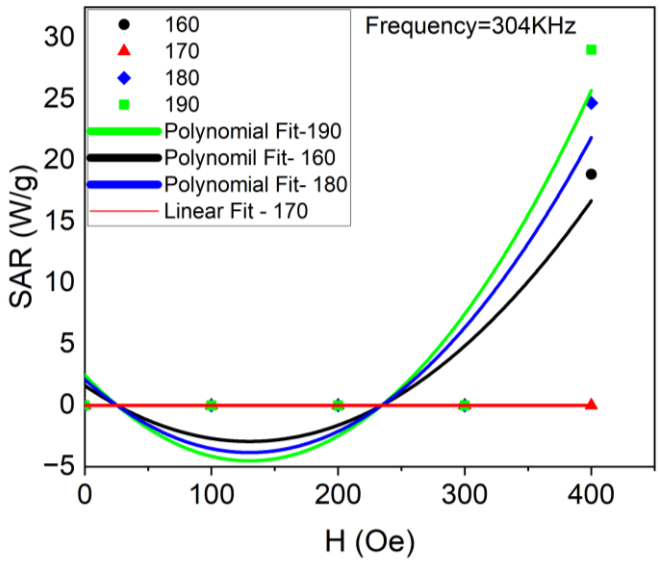

Figure 32: SAR vs. Magnetic Field measurements show an increase in SAR as the magnetic field increases from 300G to 400G.

Chapter 5: Conclusions

Iron-Silver magnetic nanoparticles were successfully synthesized using a one-pot aqueous synthesis method with different times of injection of silver at 5,7 and 9 minutes after the addition of Sodium Borohydride. Magnetic studies of the nanoparticles revealed high magnetic saturations and superparamagnetic behavior at room temperature. SEM and XRD confirm the elemental structure of the nanoparticles to be Iron Silver with an average size distribution of 30nm to 65nm. Preliminary results for hyperthermia show some temperature increase for some of the samples they interact with the AC magnetic field. It can be assumed that for the nanoparticles that did not heat up when interacting with the magnetic field could be due to lack of dispersion in water and agglomeration of the magnetic nanoparticles making it more difficult for the particles to increase in temperature.

The one-pot synthesis of Iron Cobalt magnetic nanoparticles using a modified polyol method can also be said to have been successful. By synthesizing Iron Cobalt magnetic nanoparticles at temperatures of 160℃, 170℃, 180℃ and 190℃ the magnetic properties displayed by each of them shows a pattern of increase in magnetic saturation as the temperature at which the experiment was synthesized increases. Although, for the nanoparticles synthesized at 170℃ do not follow this pattern it could be due to not removing the Ethylene Glycol properly during the cleaning process making the nanoparticles less magnetic. XRD and EDS corroborate the presence of both Iron and Cobalt in the nanoparticles. It can also be seen that the average size distribution follows an increase in size of the particles as the temperature increases except for

temperature at 190℃ where the size decreases. Hyperthermia results show an increase in temperature for three out of the four samples at a field of 400G and a frequency of 304KHz.

Treatments for Cancer have always been a case of study to find the most efficient way to attack cancer cells while also keeping the human body as healthy as possible. Specifically targeting cancer while it is its late stages can be challenging as it requires the use of chemotherapy and radiotherapy. This would reduce any kind of side effects chemotherapy would produce in patients while also getting rid of the cancer at the same time. If feasible, the use of magnetic nanoparticles to treat cancer in these late stages can provide a less invasive, safer, and better chances of giving patients a more comfortable treatment option.

List of Publications

Gasser, A., Ramadan, W., Getahun, Y., Garcia, M., Karim, M., & El-Gendy, A. A. (2023). Feasibility of superparamagnetic NIFE2O4 and go-NIFE2O4 nanoparticles for magnetic hyperthermia. *Materials Science and Engineering: B*, *297*, 116721. https://doi.org/10.1016/j.mseb.2023.116721

Garcia, M., Getahun, Y., Jansen, S., El-Gendy, A.A., Iron-Silver Magnetic Nanoparticles and their Potential use for Hyperthermia Cancer Therapy. (In Progess)

Garcia, M., Perez C., Ramirez, N., Martinez, L.A., El-Gendy, A.A., Chemical Synthesis of FeCo alloy and its feasibility for MH. (In Progress).

References

1. Bayda, S., Adeel, M., Tuccinardi, T., Cordani, M. Rizzolio, Flavio. (2019). The History of Nanotechnology: From Chemical-Physical Applications to Nanomedicine. https://www.mdpi.com/1420-3049/25/1/112

2. Park, H.-Y., Schadt, M. J., Wang, Lim, I-Im. S., Njoki, P. N., Kim, S. H., Jang, M.-Y., Luo, J., & Zhong, C.-J. (2007). Fabrication of Magnetic Core@Shell Fe Oxide@Au Nanoparticles for Interfacial Bioactivity and Bio-separation. Langmuir, 23(17), 9050–9056. https://doi.org/10.1021/la701305f

3. 2. Daniel, M.-C., & Astruc, D. (2004). Gold Nanoparticles: Assembly, Supramolecular Chemistry, Quantum-Size-Related Properties, and Applications Toward Biology, Catalysis, and Nanotechnology. ChemInform, 35(16). https://doi.org/10.1002/chin.200416213

4. 3. Gupta, A. K., & Gupta, M. (2005). Synthesis and surface engineering of iron oxide nanoparticles for biomedical applications. Biomaterials, 26(18), 3995–4021. https://doi.org/10.1016/j.biomaterials.2004.10.012

5. 4. Sounderya, N., & Zhang, Y. (2008). Use of Core/Shell Structured Nanoparticles for Biomedical Applications. Recent Patents on Biomedical Engineeringe, 1(1), 34–42. https://doi.org/10.2174/1874764710801010034

6. Ramsey, D., (2006) Safe Handling of nanotechnology

7. Rai, M., Alka Yadav, A.G., (2009). Silver nanoparticles as a new generation of antimicrobials

8. Kreuter, J., (200/). Nanoparticles=a historical perspective https://doi.org/10.1016/j.ijpharm.2006.10.021
9. Asiyanba, B., Soboyejo, W., (2008). For the Surgeon: An Introduction to Nanotechnology. https://doi.org/10.1016/j.jsurg.2007.11.006
10. Nasrollahzadeh, M.,. Sajadi, M.S., Sajjadi, M., Issaabadi, Z., (2019).Chapter 1- An Introduction to Nanotechnology. https://doi.org/10.1016/B978-0-12-813586-0.00001-8
11. 11.*The nanoscale*. Introduction to Nanotechnology. (n.d.). https://introtonanotechnology.weebly.com/the-nanoscale.html
12. Darling, S.B., Bader, S.D., (2005).A materials chemistry perpective on nanomagnetism. https://doi.org/10.1039/B506357D
13. Jiles, D. (2015). Introduction to Magnetism and Magnetic Materials. United States: CRC Press.
14. G. Bertotti*, V. Basso, C. Beatrice, M. LoBue, A. Magni, P. Tiberto(2001). Hysteresis in magnetic materials: the role of structural disorder, thermal relaxation, and dynamic effects.
15. Brandon. (2021, June 9). *What is magnetic hysteresis and why is it important?*. Materials Science & Engineering Student. https://msestudent.com/what-is-magnetic-hysteresis-and-why-is-it-important/
16. Dieckhoff, J., Eberbeck, D., Schilling, M., & Ludwig, F. (2016). Magnetic-field dependence of Brownian and néel relaxation times. *Journal of Applied Physics*, *119*(4). https://doi.org/10.1063/1.4940724

17. Dekker Encyclopedia of Nanoscience and Nanotechnology. (2004). Switzerland: M. Dekker.

18. Coey, J. M. D. (2010). Magnetism and Magnetic Materials. (n.p.): Cambridge University Press.

19. Goldman, A. (2012). Handbook of Modern Ferromagnetic Materials. Switzerland: Springer US.

20. .Anderson, P. W. (1950). Antiferromagnetism. theory of superexchange interaction. *Physical Review*, *79*(2), 350–356. https://doi.org/10.1103/physrev.79.350

21. Libretexts. (2021, September 8). *Superparamagnetism*. Engineering LibreTexts. https://eng.libretexts.org/Bookshelves/Materials_Science/Supplemental_Modules_(Materials_Science)/Magnetic_Properties/Superparamagnetism

22. Kamzin, A. S. (2016). Mössbauer investigations of Fe and FE3O4 magnetic nanoparticles for hyperthermia applications. *Physics of the Solid State*, *58*(3), 532–539. https://doi.org/10.1134/s1063783416030161

23. Chatterjee, K., Sarkar, S., Jagajjanani Rao, K., & Paria, S. (2014). Core/shell nanoparticles in biomedical applications. *Advances in Colloid and Interface Science*, *209*, 8–39. https://doi.org/10.1016/j.cis.2013.12.008

24. Deatsch, A. E., & Evans, B. A. (2014). Heating efficiency in magnetic nanoparticle hyperthermia. *Journal of Magnetism and Magnetic Materials*, *354*, 163–172. https://doi.org/10.1016/j.jmmm.2013.11.006

25. https://www.oapublishinglondon.com/article/1145

26. Karipoth, P., Thirumurugan, A., Velaga, S., Greneche, J.-M., & Justin Joseyphus, R. (2016). Magnetic properties of FeCo alloy nanoparticles synthesized through instant chemical reduction. *Journal of Applied Physics*, *120*(12). https://doi.org/10.1063/1.4962637

27. Carroll, K. J., Pitts, J. A., Zhang, K., Pradhan, A. K., & Carpenter, E. E. (2010). Nonclassical crystallization of amorphous iron nanoparticles by radio frequency methods. *Journal of Applied Physics*, *107*(9). https://doi.org/10.1063/1.3334169

28. (N.d.). *Synthesis and Stabilization of Feco Nanoparticles*. https://doi.org/10.1021/ja0708969.s001

29. Abbas, M., Nazrul Islam, Md., Parvatheeswara Rao, B., Ogawa, T., Takahashi, M., & Kim, C. (2013). One-pot synthesis of high magnetization air-stable FECO nanoparticles by modified Polyol method. *Materials Letters*, *91*, 326–329. https://doi.org/10.1016/j.matlet.2012.10.019

30. Astaraki, H., Masoudpanah, S. M., & Alamolhoda, S. (2021). Effects of ethylene glycol contents on phase formation, magnetic properties and photocatalytic activity of CUFE2O4/CU2O/cu nanocomposite powders synthesized by Solvothermal method. *Journal of Materials Research and Technology*, *14*, 229–241. https://doi.org/10.1016/j.jmrt.2021.06.046

31. Józefczak, A., Hornowski, T., Skumiel, A., Łabowski, M., Timko, M., Kopčanský, P., Koneracká, M., Szlaferek, A., & Kowalski, W. (2009). Effect of poly (ethylene glycol) coating on the magnetic and thermal properties of biocompatible magnetic liquids.

Journal of Magnetism and Magnetic Materials, *321*(10), 1505–1508. https://doi.org/10.1016/j.jmmm.2009.02.074

32. Meng, S., Yue, Z., & Li, L. (2014). Effect of ethylene glycol on the orientation and magnetic properties of barium ferrite thin films derived by chemical solution deposition. *Journal of Magnetism and Magnetic Materials*, *354*, 290–294. https://doi.org/10.1016/j.jmmm.2013.11.016
33. *Scanning electron microscopy*. Nanoscience Instruments. (2023, September 20). https://www.nanoscience.com/techniques/scanning-electron-microscopy/
34. *Vibrating sample magnetometer (VSM)*. CET Scientific Services Pte Ltd -. (n.d.). https://cet-science.com.sg/products/testing-methods/other-analysis/vibrating-sample-magnetometer-vsm/
35. *X-ray diffraction (XRD): Anton Paar Wiki*. Anton Paar. (n.d.). https://wiki.anton-paar.com/en/x-ray-diffraction-xrd/

Curriculum Vita

Marcos Adrian Garcia was born and raised in the border city of El Paso, Texas. Attended Eastlake High School and was part of the second generation to graduate from it. He later attended The University of Texas at El Paso to pursue a Bachelor of Science in Physics. Throughout his undergraduate career he had the opportunity to work as a Teaching Assistant for the Physics Department for two years. He graduated from his Bachelors in Spring of 2020 and later joined the Physics Department again to pursue a Master of Science in Physics in the Fall of 2021. As a graduate Teaching Assistant he decided to teach a new subject from what he used to teach as an undergraduate. He went on to become a TA leader for the General Physics 2 and Intro. to Electromagnetism labs during his second semester in the Master's program. He also volunteered to participate in the Physics Circus to teach students from K-12 physics concepts.

Marcos had the pleasure the join Dr. Ahmed El-Gendy's Nanoland lab during his first semester as a Master student with a focus on synthesis and characterization of magnetic nanoparticles and test their feasibility for Magnetic Hyperthermia Cancer Therapy. He was able to attend conferences such as North American-African conference where he won best poster award, SACNAS, and APS. Travel expenses were covered by the Physics Department. Under the supervision of Dr. El-Gendy he had the opportunity to collaborate in one publication, is currently working in two papers and collaborating in another. Marcos is now interested in pursuing his Doctoral degree at the University of Texas at El Paso.

Contact information: <magarcia57@miners.utep.edu>